Chapter 8
Transition Metal-Substituted Magnetite as an Innovative Adsorbent and Heterogeneous Catalyst for Wastewater Treatment

Shima Rahim Pouran, Mohammad Saleh Shafeeyan, Abdul Aziz Abdul Raman, Wan Mohd Ashri Wan Daud, and Abolfazl Bayrami

Abstract Iron oxides are conventionally used as adsorbent and/or heterogeneous catalyst because of their abundance, easy magnetically separation, affordability, and applicability in broad pH range. This is especially reported for magnetite due to the presence of Fe^{2+} cations in its structure. However, the pure magnetite has lower adsorption capacity and degradation rate in Fenton reaction, which led to the introduction of transition metal-substituted magnetite (TMSM). This section gives an overview on the adsorption potential and Fenton catalysis performance of various transition metal-substituted magnetite samples. This recently introduced group is produced with incorporation of appropriately identified transition metal/metals into the naturally available magnetite with simple synthesis method. TMSM has showed a great capacity for treating polluted water bodies using physical and chemical processes. A combination of factors affects the activity: the increased

S. Rahim Pouran (✉)
Department of Chemical Engineering, Faculty of Engineering, University of Malaya, 50603, Kuala Lumpur, Malaysia

Research Laboratory of Advanced Water and Wastewater Treatment Processes, Department of Applied Chemistry, Faculty of Chemistry, University of Tabriz, 51666-16471, Tabriz, Iran
e-mail: rahimpooran@yahoo.com; sh.rahimpooran@tabrizu.ac.ir

M.S. Shafeeyan
School of Chemical Engineering, College of Engineering, University of Tehran, 11155/4563, Tehran, Iran
e-mail: ms.shafeeyan@gmail.com

A.A. Abdul Raman • W.M.A. Wan Daud
Department of Chemical Engineering, Faculty of Engineering, University of Malaya, 50603, Kuala Lumpur, Malaysia
e-mail: azizraman@um.edu.my; ashri@um.edu.my

A. Bayrami
Department of Biology, Faculty of Basic Sciences, University of Mohaghegh Ardabili, Ardabil, Iran
e-mail: a_bayrami@uma.ac.ir

A. Bonilla-Petriciolet et al. (eds.), *Adsorption Processes for Water Treatment and Purification*, DOI 10.1007/978-3-319-58136-1_8

adsorption capacity of the samples evidenced by larger surface area, the participation of thermodynamically favorable redox pairs in regeneration of Fe^{2+} and $^{\bullet}OH$ radical generation, and the presence of oxygen vacancies serving as active sites on the surface of TMSM. Nevertheless, there is a need for further understanding and expansion of this class of adsorbents and heterogeneous catalysts.

Keywords Heterogeneous catalyst • Magnetite adsorbents • Oxidation processes • Transition metal-substituted magnetite

Contents

8.1 Introduction

Water is a key element on earth for survival of living beings, which plays a crucial role for the appropriate functioning of the terrain and aquatic ecosystems. However, water resources are contaminating continuously due to the discharge of various pollutants such as heavy metal ions, anions, dyes, organics, and microbes into the environment (Herney-Ramirez et al. 2010). Several factors including the growth in the world population, civilization, industrialization, agricultural functioning, and other geological and universal changes have contributed to the water crisis and environmental pollution (Ali and Gupta 2007). Literature reveals an increasing rate in the generation of wastewaters with refractory properties from the many of industrial activities (Shukla et al. 2010; Rahim Pouran et al. 2015b). The strategies for augmenting freshwater resources had better involved not only the prevention and minimization of water pollution but treating polluted water bodies to the degree that can be reused in another sector. In light of this, developing advanced systems for efficient water treatment and recycling have attracted considerable attention worldwide, especially in countries with a growing scarcity of water resources (Munoz et al. 2015).

Over the last decades, different approaches have been proposed and employed for water treatment, including physical methods (screening, filtration and centrifugal separation, micro- and ultrafiltration, reverse osmosis, crystallization, sedimentation and gravity separation, flotation, and adsorption), chemical methods (precipitation, coagulation, oxidation, ion exchange, and solvent extraction), electrical approaches (electrodialysis and electrolysis), thermal technologies (evaporation and distillation), and biological processes (aerobic and anaerobic processes) (Ali and Jain 2005; Diya'uddeen et al. 2015a). Out of these, adsorption is

considered as one of the practical options because of its ease of operation, low cost, and applicability for the separation of soluble and insoluble organic, inorganic, and biological contaminants (Ali 2012). Adsorption process is especially promising at nanoscale where the specific surface area of the adsorbent is relatively high. Iron oxide nanoparticles have especially attracted a wide interest due to their great magnetic characteristics that make the separation process much easier. Literature is replete with studies signifying the efficiency of iron nanomaterials as adsorbent for decontamination of heavy metal polluted aqueous solutions (Hua et al. 2012).

Nevertheless, in the most industries, the treatment methods are not able to produce effluents that comply with the effluent discharge standards (Shestakova et al. 2015). In several cases, the purification strategies basically relocate the contaminants from one phase to another (Shukla et al. 2010; Nitoi et al. 2013). Therefore, the use of such approaches is often limited due to the development of secondary wastes. For example, adsorption processes generate spent adsorbents that can be either hardly regenerated – by environmentally incompatible ex situ operating conditions – or it becomes a solid waste, commonly for industrial wastewater, that needs to be disposed (Delmas et al. 2009). The disposal of the wastes, after the water treatment process, has become a serious environmental issue that should be addressed (Diya'uddeen et al. 2015b; Shestakova et al. 2015). Consequently, advanced treatment methods are being standardized and several processes for the recovery of the spent adsorbents are being developed.

Recently, advanced oxidation processes (AOPs) have attracted a great deal of attention due to their potential for degrading numerous organic pollutants and complete mineralization of them to CO_2, H_2O, and environmentally harmless inorganic compounds, without production of secondary wastes (Comninellis et al. 2008; Wang and Xu 2011; Nichela et al. 2013). Fenton chemistry has been extensively described in recently published reviews (Pignatello et al. 2006; Malato et al. 2009). The main Fenton equations are given as Eqs. (8.1) and (8.2):

$$Fe^{2+} + H_2O_2 \rightarrow Fe^{3+} + OH^{-1} + OH^{\bullet} \tag{8.1}$$

$$Fe^{3+} + H_2O_2 \rightarrow Fe^{2+} + HO_2^{\bullet} + H^{+} \tag{8.2}$$

This process presents some advantages over the conventional approaches including simple equipment, efficient removal within a short reaction time, and potential for complete oxidation and mineralization of contaminants to benign end products under appropriate operational conditions. The Fenton reaction initiated by heterogeneous Fe^{2+} or Fe^{3+} compounds or some other transition metals at low oxidation states such as Co^{2+} and Cu^{2+} is referred as Fenton-like reaction (Nichela et al. 2013). Fenton-like reaction (Eq. 8.2) has a lower rate compared to Fenton reaction (Eq. 8.1) (0.01–0.002 vs. 42–79 L/mol S) due to the unbound transfer of the reactants in the homogeneous reaction site. The relative abundance and low cost of iron minerals as well as their simple magnetic separation render them as suitable candidates as adsorbents and for heterogeneous Fenton treatment of recalcitrant wastewaters. Accordingly, several researchers have focused on improving the

efficiency of iron oxides and enhancing the breakdown rate of contaminant molecules through structural modifications.

One of the recently studied alterations is to substitute the structural iron species of iron minerals with other active transition metals. The effectiveness of transition metal-substituted magnetite (TMSM) as an innovative adsorbent and heterogeneous catalyst for water treatment is presented in the following sections.

8.2 Transition Metal-Substituted Magnetite

Magnetite is the most dominant iron mineral that has been employed for TMSIO synthesis. Iron in the magnetite structure can be substituted isomorphically by other transition metals, wherein the integrated transition metal/metals should have similar ionic radius to Fe^{2+}/Fe^{3+} cations and the same or with one or two unit differences in the oxidation states to the exchanged iron species. For instance, magnetite octahedral Fe^{3+} is replaced by Cr^{3+} in $Fe_{3-x}Cr_xO_4$ with the similar ionic radii (64.5 vs. 61.5 pm) (Magalhães et al. 2007) and Fe^{3+} is replaced by Nb^{5+} with the same ionic radius (64 pm) (Oliveira et al. 2008; Rahim Pouran et al. 2015a). Concerning the replacements with differing charges, the same amount of Fe^{3+} is reduced to Fe^{2+} based on the electrovalence equilibrium (Pearce et al. 2015). On the other hand, the structural dislocations could be adjusted by prompting oxygen vacancies for the substitutions in the absence of reduction (Moura et al. 2006). These oxygen vacancies are believed that perform as active sites for generation of hydroxyl radicals in Fenton process.

The most widely used preparation approach is the coprecipitation of highly pure ferrous and ferric salts (Fe^{2+}/Fe^{3+} in the molar ratio of 1:2) plus a predetermined amount of the selected transition metal salt under an inert gas environment and a few drops of hydrazine to prevent the oxidation of ferrous cations (Fig. 8.1) (Yang et al. 2009a; Liang et al. 2012b). This process can be continued by thermal treatment at 400–430 °C (Costa et al. 2003, 2006; Lelis et al. 2004).

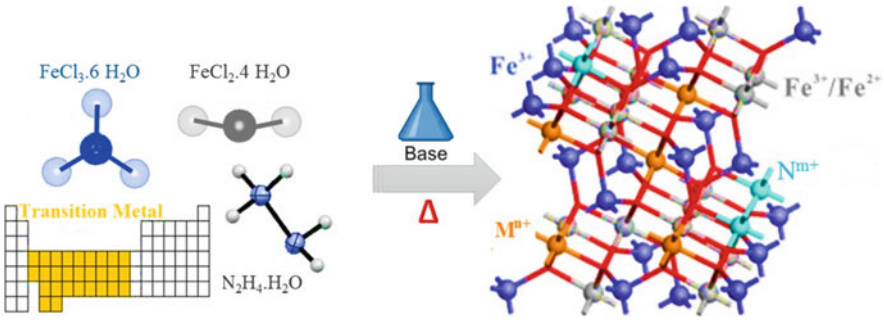

Fig. 8.1 Coprecipitation of Fe^{2+}, Fe^{3+}, and M^{n+} and/or N^{m+} as a TMSM

Yang et al. (2009a) represented the following set of reactions (Eqs. (8.4), (8.5), (8.6), and (8.7)) involved in synthesis of $Fe_{3-x}Ti_xO_4$ that were considered by Sugimoto and Matijević (1980):

$$(3-x)Fe^{2+} + xTi^{4+} + (6+2x)OH^- \rightarrow Fe_{3-x}Ti_x(OH)_{6+2x} \tag{8.3}$$

$$Fe_{3-x}Ti_x(OH)_{6+2x} + (1-x)NO_3^- \rightarrow Fe_{3-x}Ti_xO_4 + (1-x)NO_2^- + (3+x)H_2O \tag{8.4}$$

$$Fe_{3-x}Ti_x(OH)_{6+2x} + (2-2x)NO_2^- \rightarrow Fe_{3-x}Ti_xO_4 + (2-2x)NO + (2+2x)H2O + (2-2x)OH^{-1} \tag{8.5}$$

$$5Fe_{3-x}Ti_x(OH)_{6+2x} + (2-2x)NO \rightarrow 5Fe_{3-x}Ti_xO_4 + (2-2x)NH_3 + (8x+12)H_2O \tag{8.6}$$

TMSIOs of other iron oxides are often prepared under air atmosphere (dos Santos et al. 2001; Alvarez et al. 2006; Guimaraes et al. 2009) because they only contain Fe^{III} species. Meanwhile, the preparation procedure, type and quantity of the loaded transition metal, and the temperature range influence the properties of the developed TMSIO. The preparation of different catalysts through the impregnation of magnetite with transition metal/metals has been extensively reported in the literature. Most of the studies have explored the incorporation of the period 4 transition metals such as Ti (Yang et al. 2009a, b; Liang et al. 2012a, b; Zhong et al. 2012), V (Liang et al. 2010, 2012b), Cr (Magalhães et al. 2007), Mn (Oliveira et al. 2000; Costa et al. 2003, 2006; Coker et al. 2008), Co (Costa et al. 2003, 2006; Lelis et al. 2004; Coker et al. 2008), Ni (Costa et al. 2003, 2006; Coker et al. 2008), Cu (Lee and Joe 2010), Zn (Coker et al. 2008), and other metals like Al (Jentzsch et al. 2007) into the magnetite structure. The schematic presentation of the preparation set up is shown in Fig. 8.2.

The investigation on the recent studies indicates that this group of chemicals can be proposed as a novel promising adsorbent and heterogeneous Fenton catalyst in the degradation of organic pollutants.

8.3 Physicochemical Changes in Modified Magnetite

The incorporated transition metal may give rise to significant changes in magnetite physicochemical properties (Magalhães et al. 2007; Zhong et al. 2012). The main structural changes in magnetite structure through the incorporation of various transition metals are given in Table 8.1. The degree of advancement in physicochemical properties is mainly dependent on the synthesis method, type and percentage of the host metal/metals, and nature of the occupied site (Oliveira et al. 2000; Ramankutty and Sugunan 2002; Costa et al. 2003; Magalhães et al. 2007; Lee et al. 2008; Zhong et al. 2012; Liang et al. 2013). Nonetheless, the spinel structure of magnetite is often kept unchanged after the incorporation.

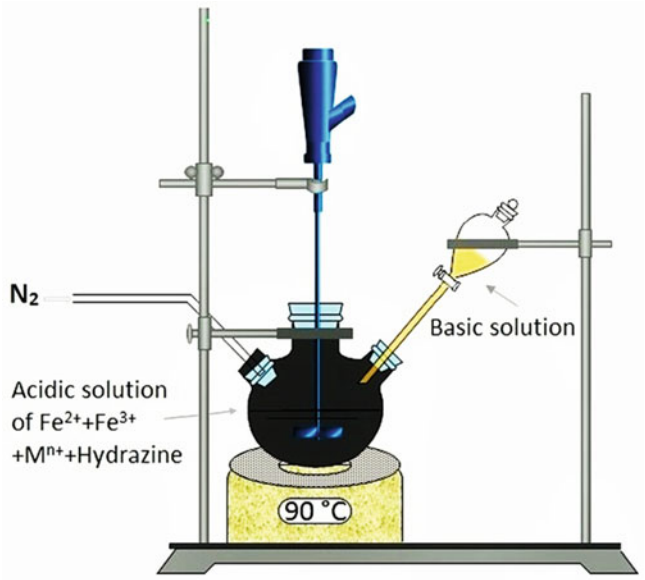

Fig. 8.2 The schematic presentation of the TMSM preparation set up (Rahim Pouran et al. 2015c)

Several literature on the characteristics of TMSM samples using Brunauer-Emmett-Teller (BET) surface area analysis reported a major growth in the surface area, primarily caused by a decrease in the particle size and/or pore diameter (Silva et al. 2009; de Souza et al. 2010; Liang et al. 2012b; Zhong et al. 2012). For example, in the $Fe_{2.93}Cr_{0.07}O_4$ sample, the pore diameter decreased from meso- to micro-size via the substitution of Fe^{3+} by Cr^{3+} in which the surface area was significantly increased (Magalhães et al. 2007). On the other hand, there was indistinct variation in the surface area and porosity of magnetite after the incorporation of Al, as reported by Jentzsch et al. (2007). It is worth mentioning that the magnetic property of magnetite should be preserved after the modification, as it is required for facile recovery of the sample from the treated water (Liang et al. 2012b). This characteristic can be affected by the cationic arrangement in the tetrahedral and octahedral sites, production condition, and the size of magnetite (Lelis et al. 2004). For instance, a decrease in the particle size to a few nanometers can intensify the magnetic order on the surface of the magnetite particles (Haneda and Morrish 1988).

8.4 Adsorption

Surface characteristics of a hetero-catalyst define its activity in a solution. The electrostatic interaction between the probe molecule and the catalyst surface is a major controlling parameter, so that the probe molecule removal from the target

Table 8.1 Preparation method and characteristics of transition metal-substituted iron oxide catalysts (Rahim Pouran et al. 2014)

Heterogeneous catalyst	Characteristics	Preparation method	References
$Fe_{3-x}Cr_xO_4$ (x = 0.00, 0.07, 0.26, 0.42, and 0.51) Fe_3O_4 $Fe_{2.93}Cr_{0.07}O_4$ $Fe_{2.74}Cr_{0.26}O_4$ $Fe_{2.58}Cr_{0.42}O_4$ $Fe_{2.49}Cr_{0.51}O_4$	Spinel crystalline, replacing Cr^{3+} by Fe^{3+}_{oct} and for higher Cr contents by Fe^{2+}_{oct} and Fe^{3+}_{tet}, substitution by Cr^{3+} decreased the pore diameter from meso- to micropore with a significant increase on the BET surface area	Conventional coprecipitation method	Magalhães et al. (2007)
$Fe_{3-x}Ti_xO_4$ (x = 0.00, 0.20, 0.46, 0.71, and 0.98) Fe_3O_4 $Fe_{2.80}Ti_{0.20}O_4$ $Fe_{2.54}Ti_{0.46}O_4$ $Fe_{2.29}Ti_{0.71}O_4$ $Fe_{2.02}Ti_{0.98}O_4$	Well-crystallized spinel structure, contains Ti^{4+} in octahedral sites, hydrophilic surface, decrease in particle size (≈82 nm) and pore diameter plus significant increase in surface area along with the increase in Ti content	Precipitation-oxidation method	Zhong et al. (2012)
$Fe_{3-x}Mn_xO_4$ (x = 0.21, 0.26, and 0.53) Fe_3O_4 $Fe_{2.79}Mn_{0.21}O_4$ $Fe_{2.74}Mn_{0.26}O_4$ $Fe_{2.47}Mn_{0.53}O_4$	Existence of the spinel phase, Mn^{2+} replacing mainly Fe^{2+} in the octahedral site, i.e., $[Fe^{3+}]_{tetrahedral}\left[Fe^{3+}Fe^{2+}_{1-x}M^{2+}_x\right]_{octahedral}O_4$, phase transformation of magnetite to maghemite and hematite due to the presence of Mn	Coprecipitation of the precursor ferric hydroxyl-acetate containing the metal Mn	Costa et al. (2003, 2006), Oliveira et al. (2000)
$Fe_{3-x}Co_xO_4$ (x = 0; 0.19; 0.38 and 0.75) Fe_3O_4 $Fe_{2.81}Co_{0.19}O_4$ $Fe_{2.62}Co_{0.38}O_4$ $Fe_{2.25}Co_{0.75}O_4$	Existence of the spinel phase, Co^{2+} replacing mainly Fe^{2+} in the octahedral site, i.e., $[Fe^{3+}]_{tetrahedral}\left[Fe^{3+}Fe^{2+}_{1-x}M^{2+}_x\right]_{octahedral}O_4$, the increase in hyperfine magnetic field for the octahedral iron with the increase in structural Co	Coprecipitation of the precursor ferric hydroxyl-acetate containing the metal Co	Costa et al. (2003, 2006), Lelis et al. (2004)

(continued)

Table 8.1 (continued)

Heterogeneous catalyst	Characteristics	Preparation method	References
$Fe_{3-x}Ni_xO_4$ (x = 0; 0.10; 0.28 and 0.54) Fe_3O_4 $Fe_{2.90}Ni_{0.10}O_4$ $Fe_{2.72}Ni_{0.28}O_4$ $Fe_{2.46}Ni_{0.54}O_4$	Existence of the spinel phase, Ni^{2+} replacing mainly Fe^{2+} in the octahedral site, i.e., $[Fe^{3+}]_{tetrahedral}\left[Fe^{3+}Fe^{2+}_{1-x}M^{2+}_{x}\right]_{octahedral}O_4$	Coprecipitation of the precursor ferric hydroxyl-acetate containing the metal Ni	Costa et al. (2003, 2006)
$Fe_{3-x-x'}Ti_xV_{x'}O_4$ (x = 0.00, 0.40, 0.42, 0.54, and 0.69) ($x' = 0.00, 0.03, 0.08, 0.13$, and 0.32) Fe_3O_4 $Fe_{2.31}Ti_{0.69}O_4$ $Fe_{2.43}Ti_{0.54}V_{0.03}O_4$ $Fe_{2.50}Ti_{0.42}V_{0.08}O_4$ $Fe_{2.47}Ti_{0.40}V_{0.13}O_4$ $Fe_{2.68}V_{0.32}O_4$	Well-crystallized spinel structure, occupancy of mainly octahedral sites by Ti^{4+} and V^{3+}, no apparent effect of Ti-V on the magnetite structure, size: less than 100 nm, magnetic, higher adsorption activity of Ti-V magnetite catalysts than pure magnetite (more dependent on Ti than V), increase in specific surface area compared to Fe_3O_4	Coprecipitation method	Liang et al. (2012b)
$Fe_{3-x}Ti_xO_4$ (x = 0.00, 0.17, 0.23, 0.37, 0.50, 0.78) Fe_3O_4 $Fe_{2.83}Ti_{0.17}O_4$ $Fe_{2.77}Ti_{0.23}O_4$ $Fe_{2.63}Ti_{0.37}O_4$ $Fe_{2.50}Ti_{0.50}O_4$ $Fe_{2.22}Ti_{0.78}O_4$	Spinel structure, bigger lattice parameter than magnetite, average diameters of 120 nm, Ti^{4+} replacing mainly Fe^{3+} in the octahedral site. Simultaneous increase in oxidation and transition temperature by increase in Ti content, increase in surface area from 6.65 $m^2\ g^{-1}$ of pure magnetite to 20.7 $m^2\ g^{-1}$ in titanomagnetite	New soft chemical method	Yang et al. (2009a, b)

$Fe_{3-x}V_xO_4$ (x = 0.00, 0.16, 0.26, 0.34) $Fe^{2+}_{0.61}Fe^{3+}_{2.39}O_4$ $Fe^{2+}_{0.45}Fe^{3+}_{2.39}V_{0.16}O_4$ $Fe^{2+}_{0.70}Fe^{3+}_{2.04}V_{0.26}O_4$ $Fe^{2+}_{0.73}Fe^{3+}_{1.93}V_{0.34}O_4$	V^{3+} mainly occupies the octahedral site (chiefly replaced Fe^{3+}), the increase in vanadium content causes a decrease in the total Fe and Fe^{3+} content, no apparent change in the average crystal size and surface area, increase in the superficial hydroxyl groups, and a decrease in the temperature of maghemite-hematite phase transformation	Precipitation-oxidation method	Liang et al. (2010)
$Fe_{3-x}Al_xO_4$ (x = 0.00, 1.48, 2.14, 5.49, 8.07 mol %) Fe_3O_4 $Fe_{2.83}Al_{0.17}O_4$ $Fe_{2.77}Al_{0.23}O_4$ $Fe_{2.63}Al_{0.37}O_4$ $Fe_{2.50}Al_{0.50}O_4$	Al^{3+} replacing mainly Fe^{3+}, the increase in aluminum content causes a decrease in the particle size, no obvious change in porosity of the particles and their surface area, samples containing greater amounts of aluminum were overall less reactive than undoped samples	Coprecipitation method	Jentzsch et al. (2007)
$Cu_xFe_{3-x}O_4$ (x = 0.00, 0.2, 0.3) Fe_3O_4 $Cu_{0.2}Fe_{2.8}O_4$ $Cu_{0.3}Fe_{2.7}O_4$	A single-phase cubic spinel structure of $Cu_{0.2}Fe_{2.8}O_4$ in magnetite and $Cu_{0.3}Fe_{2.7}O_4$, consists of a cubic spinel structure in magnetite and a hexagonal structure in hematite	Mechanical alloying	Lee and Joe (2010)

solution is largely determined by its adsorption on the catalyst surface (Yang et al. 2009b). Several factors such as contact time, pH, chemical properties, and initial concentration of contaminant affect the adsorption capacity of the catalyst (Hanna et al. 2008; Yang et al. 2009b; Ai et al. 2011a; Yuan et al. 2011; Liang et al. 2012a). Among surface properties, basicity is an important factor that arises from the hydroxyl groups on the surface of the catalyst. The ligand shell accomplishment of the surface Fe atoms leads to the formation of Fe-OH groups on surface of the catalysts in which the surface adsorption is largely controlled by these groups (Sun et al. 1998). Accordingly, pH plays a dominant functional role in the catalytic action of the iron oxides. The pH of point of zero charge (PZC) is a key parameter that is defined as the pH in which the charge of the surface of the iron oxide is zero or the total number of the $FeOH^{2+}$ and FeO^{-} groups on the catalyst surface is the same. Conventionally, the determination of the pH_{pzc} is crucial for identifying the solution pH influence on the catalyst surface charge and consequent interaction with probe molecule.

In magnetite, protonation and deprotonation are the main reactions that occur on the surface, which are given by Eqs. (8.7), (8.8), and (8.9):

$$\equiv \mathrm{Fe(II-III)} \sim \mathrm{OH} + \mathrm{H^+} \leftrightarrow \mathrm{Fe(II-III)} \sim \mathrm{OH_2^+} \quad \mathrm{pH} < \mathrm{pH_{pzc}} \tag{8.7}$$

$$\equiv \mathrm{Fe(II-III)} \sim \mathrm{OH} \leftrightarrow \mathrm{Fe(II-III)} \sim \mathrm{O^-} + \mathrm{H^+} \quad \mathrm{pH} > \mathrm{pH_{PZC}} \tag{8.8}$$

$$\equiv \mathrm{Fe} \sim \mathrm{OH} + \mathrm{OH^-} \rightarrow \mathrm{Fe} \sim \mathrm{O^-} + \mathrm{H_2O} \quad \mathrm{pH} > \mathrm{pH_{pzc}} \tag{8.9}$$

At higher pH values than pH_{pzc}, the magnetite surface is negatively charged, and at lower pH values, it is positive (Petrova et al. 2011). The pH_{pzc} of magnetite at room temperature changes between 6.0 and 6.8 in an aqueous medium wherein the surface charge is of about neutral at this range (Sun et al. 1998; Cornell and Schwertmann 2003). Accordingly, the surface of the magnetite samples is negatively charged at pH higher than pH_{pzc}. Hence, it is favored for the adsorption of cationic probe molecules such as methylene blue (MB), based on the electrostatic interaction, and vice versa. For example, Liang et al. (2012a) observed that MB removal through Fenton reaction catalyzed by Cr-substituted magnetite was significantly influenced by its adsorption on the sample surface at neutral pH value, whereas the samples indicated no adsorption to acid orange II (anionic dye) and the degradation of the investigated dyes demonstrated different removal mechanisms. Table 8.2 gives a number of examples on the modified magnetite adsorbents for eliminating various contaminants from the aqueous medium. The data shows that the adsorption is highly affected by the pH of the solution.

In the heterogeneous catalysis, the iron catalyst and the organic pollutant are stirred together for a period of time to achieve the adsorption equilibrium (Hanna et al. 2008). The maximum adsorption is normally attained in the first hour and it continues at a decreased rate to reach the equilibrium state. It can be ascribed to the progressive filling of the most active adsorption sites on the catalyst surface. Then, the adsorption rate decreases as a result of the decreased vacant sites and subsequent repulsion force between the catalyst surface and adsorbed molecules.

Table 8.2 Iron oxide-based adsorbents for contaminant removal through adsorption

Compound/initial amount (mg/L)	Adsorbent	Operational condition					Optimal performance	References
		Contact time (min)	pH_{pzc}	Solution pH	T (°C)	Shaking speed (rpm)		
Methylene blue (MB)/20	(M-MWCNTs)[1] 0.02 g/50 ml	120	6.5	2–10	25 ± 1	150	The adsorption capacity of MB increases with increasing solution pH from 2.0 to 7.0 and changes slightly when solution pH is above 7.0. Adsorption kinetics follows the pseudo-second-order model. Maximum monolayer adsorption capacity: 48.06 mg g^{-1}	Ai et al. (2011a)
Methyl orange (MO)/4.8	Mg-Al LDH[2]	50		5.0	25	> 420	The adsorption capacity of the Mg-Al LDH toward MO was 0.453 mol/kg. The adsorption kinetics and equilibrium adsorption data were well-described by the pseudo second order model and fitted well to both the Langmuir and Freundlich models, respectively	Ai et al. (2011b)
Cd^{2+}/100	P (MB-IA)-g-MNCC[3] 2 g/L	240	6.1	8.0	30	200	The maximum adsorption capacity of P (MB-IA)-g-MNCC was found to be 262.27 mg/g. Kinetic and isotherm data were described using pseudo-second-order kinetic model and Sips isotherm model, respectively	Anirudhan and Shainy (2015)
P/40	Magnetic iron oxide (MIO) 1 g/50 ml	120	5.8	> 5.0	35	NA	The maximum adsorption capacity of MIO was 15.2 mg P/g MIO. The adsorbed phosphorous was effectively detached from MIO within 30 min using 20 wt% NaOH solution. The adsorption kinetic of the phosphate adsorption on MIO fitted well on the pseudo-second-order and Elovich models	Choi et al. (2016)

(continued)

Table 8.2 (continued)

Compound/initial amount (mg/L)	Adsorbent	Operational condition					Optimal performance	References
		Contact time (min)	pH_{pzc}	Solution pH	T (°C)	Shaking speed (rpm)		
Cd^{2+}/44.6	MT-MN 0.53 g	240	NA	3.5	20	120	The maximum adsorption capacity of the MN-MT for Cd^{2+} was 52.05 mg g^{-1}. Kinetic studies revealed that the adsorption process followed the pseudo-second-order model	Guyo et al. (2015)
Cu^{2+}, Pb^{2+}, Cd^{2+}, Cr^{6+}, Ni^{2+}, 20 each	NMag-CS 2 g/L	120	NA	5.5	25	200	96% Cu^{2+} and 94.6 Cr^{6+}, Pb^{2+}, Cd^{2+}, and Ni^{2+} removal percentage on film surface. The adsorption data were well fitted by both the Langmuir and Freundlich isotherms and the pseudo-second-order kinetics	Lasheen et al. (2016)
Pb^{2+}	Mn-magnetite 1 g/L	60	7.1	4.5	25	600	The adsorption capacity of magnetite samples toward Pb (II) gradually increased with the increase in Mn content. The adsorption capacity q_m for the samples with C_{Mn} 20 Wt % was 36.27 mg g^{-1}	Liang et al. (2014)
Cr^{6+} and Pb^{2+}/50 each	Fe_3O_4 NP	Up to 24 h	7.4	2 and 5	45	NA	The Sips and Langmuir models best described Cr^{6+} and Pb^{2+} adsorption on magnetite nanoparticles, respectively. The maximum Langmuir adsorption capacities were 34.87 (Cr^{6+}) and 53.11 (Pb^{2+}) mg/g. The pseudo-second-order model fits the adsorption kinetics	Rajput et al. (2016)

Cr^{6+}/50	MMT-Mag NP 0.5 g/100 ml	120	8.3	2–2.5	25 ± 2	160	Kinetics of the adsorption followed the pseudo-second-order model. Adsorption data fit well with the Langmuir and Freundlich isotherm equations. Adsorption capacity per unit mass of magnetite: 15.3 mg/g	Yuan et al. (2009)

M-MWCNTs are magnetite-loaded multi-walled carbon nanotubes. Mg-Al LDH is layered double hydroxide. P (MB-IA)-g-MNCC is 2-mercaptobenzamide modified itaconic acid-grafted-magnetite nanocellulose composite. MT-MN is maize tassel-magnetite nanohybrid. NMag-CS is nano-magnetite chitosan film. MMT-Mag NP is montmorillonite-supported magnetite nanoparticles

In a study conducted by Liang et al. (2012b), the substitution of Ti^{4+} and V^{3+} improved the adsorption activity of magnetite such that all the $Fe_{3-x-x'}Ti_xV_{x'}O_4$ samples had greater saturated adsorbed content than Fe_3O_4 with much higher dependence on the amount of Ti^{4+} than V^{3+}. Similarly, $Fe_{3-x-y}Nb_xMo_yO_4$ samples showed a significantly higher adsorption capacity of 80% more than the pure magnetite in which the effects of Nb incorporation were prominent (Rahim Pouran et al. 2015c). This clearly indicates that the incorporation of transition metals positively affected the magnetite adsorption capacity, primarily resulting from the enlarged specific surface area and, accordingly, the amount of magnetite surface hydroxyl (Liang et al. 2014).

On the other hand, the adsorption kinetics provides valuable understanding of the reaction pathways and the adsorption mechanism and describes the solute uptake rate. A number of models can be employed to express the mechanism of solute adsorption onto a sorbent. To explore the adsorption mechanism, a pseudo-first-order equation of Lagergren (1898) based on solid capacity, a first-order equation of Bhattacharya et al. (1984) based on solution concentration, and a pseudo-second-order equation based on solid phase adsorption rate are used to determine the characteristic constants of adsorption. Details of both models are provided in Chap. 3.

The pseudo-first-order model proposes that the experimental data is only well fitted to an initial period of the first reaction step. However, the pseudo-second-order model provides the best correlation of the experimental data over a long period in the studied systems (Ho and McKay 1999). Consequently, in the most adsorption studies using modified magnetite samples, the adsorption kinetics were well described by pseudo-second-order model in kinetics (Table 8.2). For instance, in a study on the MB adsorption on co-substituted Nb-Mo-magnetite samples, the pseudo-second-order model presented the best fit to the kinetic data at 25, 50, 100, and 200 mg L^{-1} MB concentrations (Rahim Pouran et al. 2015c). However, it should be borne in mind that the kinetic models are not adequate to describe the adsorption process. Indeed, adsorption is a complex multistep process, and the kinetic studies provide valuable insights of the adsorption mechanisms which involve mass transfer, diffusion, and surface reaction phenomenon. In addition to the kinetic studies, it is recommended to investigate the adsorption data using various isotherm models and thermodynamic evaluations. Lastly, the merits accompanied the adsorption process, such as easy operation, low cost, and huge sludge-handling processes could be completed with a more efficient method that helps for effective contaminant removal. Heterogeneous Fenton process is an excellent candidate for this purpose.

8.5 Oxidation Process

Transition metal-substituted magnetite (TMSM) has received growing interest for treatment of wastewaters using Fenton reaction, due to their higher adsorption capacity and reactivity in the degradation reaction compared to pure magnetite

(Rahim Pouran et al. 2014). The degradation process is started by adsorption of contaminant molecules on the catalyst surface before H_2O_2 addition and starting Fenton reaction.

From the reports, the enhancement in the catalytic activity of the modified magnetite samples has been resulted from the existence of the thermodynamically favorable redox pairs of the imported cations on the surface of the catalysts. These redox pairs enhance the Fenton degradation of probe molecule via (i) direct involvement in Fenton oxidation cycle and generation of $^{\bullet}OH$ radicals through Haber-Weiss mechanism, (ii) regeneration of Fe^{+2} cations, and (iii) acceleration of the electron transfer during the oxidation reaction in the magnetite structure (Costa et al. 2003).

Generation of oxygen vacancies from the adjustments for unequal charge replacements or cationic deficiency in the structure of modified iron oxide was proposed by Costa et al. (2006) as another possible reason for enhanced activities. These vacancies act as active sites in which they directly get involved in the degradation of probe molecules or indirectly in decomposition of H_2O_2 (Magalhães et al. 2007).

In photocatalysis process, the incorporated transition metals prevent the recombination of the photo-excited holes (h^+) and electrons (e^-) on the catalyst surface (Büchler et al. 1998) and extend the existence time of the charge carriers. For illustration, Fig. 8.3 shows the action of substituted Nb and Mo in magnetite samples for oxidation of MB (Rahim Pouran et al. 2015c). Other parameters including enlarged surface area and, accordingly, higher concentrations of OH groups on the surface of the catalysts are also reported in a number of studies (Liang et al. 2012a). However, the type and the quantity of probe molecule, Fenton reagent concentration, reaction duration and condition, and more importantly the elemental ratio of the imported transition metal play influential role in the

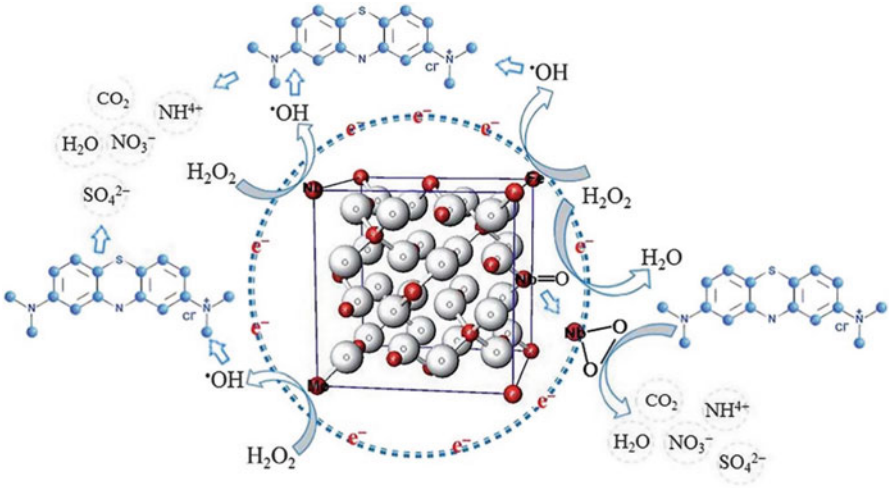

Fig. 8.3 Action of substituted Nb and Mo in magnetite samples for oxidation of MB through Fenton reaction (Rahim Pouran et al. 2015c)

degradation efficacy. For example, Costa et al. (2006) reported that although MB (50 ppm) removal was achieved within 10 min, the higher H_2O_2 concentrations (0.3 M) and Co (x = 0.75) and Mn (x = 0.53) loads were the major causes of the short reaction time. Liang et al. (2012a) observed that 59.3% of MB (≈64 mg L^{-1}) was oxidized using the $Fe_{2.82}Cr_{0.18}O_4/H_2O_2$ (0.08 M) within 4 h, whereas $Fe_{2.33}Cr_{0.67}O_4/H_2O_2$ resulted in 95% color removal within the same reaction time. Furthermore, a long time of reaction (11 h) was utilized to degrade more than 90% of MB (70 mg g^{-1} of $Fe_{2.66}V_{0.34}O_4$ at pH 10 (Liang et al. 2013). On the contrary, the $Fe_{2.79}Nb_{0.171}Mo_{0.023}O_4$ catalyzed Fenton reaction could remove 100 mg/L of MB within 150 min (Rahim Pouran et al. 2015c), whereas the degradation was about 80% using $Fe_{2.73}Nb_{0.19}O_4$ sample (Rahim Pouran et al. 2015a).

The optimum portion of the integrated active cation to iron species drives higher activities and a concentration above this value may not improve the activity. For instance, Yuan et al. (2011) reported that the highest degradation percentage of dimethyl phthalate (DMP) by Si = FeOOH was detected at Si/Fe ratio of 0.2; however, this percentage decreased at lower and higher values than 0.2. It can be ascribed to the generation of suspended indigent catalyst at lower ratios and subsequent decrease in UV transmission into the solution. At higher values, the active sites are masked with high SiO_2 concentrations and lead to the formation of lower hydroxyl radical from H_2O_2 breakdown. Nevertheless, the increment in the content of the integrated Co and Mn leads to a remarkable increase in the catalyst activity where Fe_3O_4 demonstrated lower activity in comparison with the $Fe_{3-x}Co_xO_4$ and $Fe_{3-x}Mn_xO_4$ catalysts. In this study, the $Fe_{2.25}Co_{0.75}O_4$ and $Fe_{2.47}Mn_{0.53}O_4$ had the highest activities in the aforementioned reactions (Costa et al. 2003).

A combination of iron oxides and natural niobia (Nb_2O_5) led to the generation of a composite catalyst, of which maghemite (γFe_2O_3) and goethite (αFeOOH) were the chief constituents in its structure (Oliveira et al. 2007). The niobia load of the composite significantly influenced the discoloration rate, of which the niobia/iron oxide ratio of 1:5 only removed the half of the MB in solution, whereas in ratio of 1:1, the removal percentage was approximately 90%. Table 8.3 summarizes the data on the degradation of recalcitrant organic compounds using transition metal-substituted magnetite catalysts in Fenton reactions.

8.6 Conclusions

The research on magnetite as an adsorbent has been increasing due to its applicability in a wide range of pH, easy separation, and reusability. However, the adsorption capacity of magnetite can be improved via modification in its structure by enhancing its specific surface area and surface properties. One of the most promising methods that enhances its adsorption characteristic is the isomorphic substitution of the structural iron of magnetite with other transition metal/metals.

Table 8.3 Oxidation of various organic pollutants through Fenton reactions catalyzed by transition metal-substituted iron oxide (Rahim Pouran et al. 2014)

Compound	Catalyst	Operational condition				Optimal performance	References
		$[H_2O_2]$	pH	T (°C)	λ (nm)		
Methylene blue [MB], 50 mg/L	Cr-magnetite $Fe_{3-x}Cr_xO_4$ (15 mg)	0.3 mg/L	6.0	25	–	Higher degradation rate at lower Cr content, decrease in discoloration rate, and TOC removal by increase in Cr content mainly due to the decrease in Fe^{2+}	Magalhães et al. (2007)
Tetrabromobis-phenol A [TBBPA], 20 mg/L	Titanomagnetite $Fe_{2.02}Ti_{0.98}O_4$ 0.125 g L^{-1}	10 mmol/L	6.5	25	–	>97% TBBPA degradation in UV/$Fe_{2.02}Ti_{0.98}O_4$/H_2O_2 system, ≈75% in UV/H_2O_{2tr} system within 240 min of UV irradiation	Zhong et al. (2012)
Methylene blue [MB], 100 mg/L	$Fe_{2.46}Ni_{0.54}O_4$ $Fe_{2.47}Mn_{0.53}O_4$ $Fe_{2.25}Co_{0.75}O_4$ (30 mg)	2.5 mol/L	–	25	633	10% color removal within 50 min using $Fe_{2.46}Ni_{0.54}O_4$, complete discoloration of the solution in 5 and 10 min using $Fe_{2.47}Mn_{0.53}O_4$ and $Fe_{2.25}Co_{0.75}O_4$, respectively	Costa et al. (2003)
Chlorobenzene [CBZ], 30 mg/L	Mn-magnetite $Fe_{3-x}Mn_xO_4$ (30 mg)	2.5 mol/L	–	25	–	14, 7, 5, and <1% chlorobenzene degradation for the reactions using $Fe_{2.47}Mn_{0.53}O_4$, $Fe_{2.74}Mn_{0.26}O_4$, $Fe_{2.79}Mn_{0.21}O_4$, and Fe_3O_4, respectively	Oliveira et al. (2000), Costa et al. (2003)
Methylene blue [MB], 100 mg/L	γ-Fe_2O_3 α- Fe_2O_3 $Fe_{3-x}M_xO_4$ (M = Co and Mn) (30 mg)	0.3 mol/L (10 mL)	5–6.5	25	–	Not remarkable discoloration with Fe_2O_3 oxides, complete color removal, and higher oxidation by $Fe_{3-x}M_xO_4$ within 5–10 min	Costa et al. (2006)
Chlorobenzene [CBZ], 20 mg/L	Mn-magnetite $Fe_{3-x}Mn_xO_4$ (30 mg)	0.3 mol/L	–	25	–	1, 5, 7, and 14% CBZ removal using Fe_3O_4, $Fe_{2.79}Mn_{0.21}O_4$, $Fe_{2.74}Mn_{0.26}O_4$, and $Fe_{2.47}Mn_{0.53}O_4$, respectively, within 30 min	Costa et al. (2006)

(continued)

Table 8.3 (continued)

Compound	Catalyst	Operational condition				Optimal performance	References
		$[H_2O_2]$	pH	T (°C)	λ (nm)		
Methylene blue UV [MB], 0.2 mmol/L (500 mL)	Ti-V-magnetite $Fe_{3-x-x'}Ti_xV_{x'}O_4$ (1.0 g/L)	10 mmol/L	7.0	25	365	Increase in MB discoloration from 48% to 96% by increase in Ti content from x = 0.0 to x = 0.69 after 120 min	Liang et al. (2012b)
Methylene blue [MB], 100 mg/L (400 mL)	Titanomagnetite $Fe_{3-x}Ti_xO_4$ (1.0 g/L)	0.30 mol/L	6.8	30	–	Higher activity for Ti-magnetite than pure magnetite, decrease in residual MB with the increase in Ti content	Yang et al. (2009a, b)
Methylene blue [MB], 100 mg L^{-1} (150 mL)	Nb-magnetite Mo-magnetite Nb-Mo-magnetite (1.0 g/L)	0.2 mol/L	7.0	25	–	Higher activity for modified magnetite than pure magnetite; co-substituted Nb-Mo-magnetite had the highest activity compared to single metal-substituted samples. Decrease in residual MB with the increase in Nb content compared to Mo	Rahim Pouran et al. (2015a, c)
Methylene blue [MB], 0.2 mmol/L (200 mL)	V-magnetite $Fe_{3-x}V_xO_4$ $0 \leq x \leq 0.34$ (1.0 g/L)	100 mmol/L	10.0	25	–	Color removal of 41, 60, 81, and 93% of MB within 11 h using Fe_3O_4, $Fe_{2.84}V_{0.16}O_4$, $Fe_{2.74}V_{0.26}O_4$, and $Fe_{2.66}V_{0.34}O_4$, respectively	Liang et al. (2010)
Methylene blue [MB], 50 mg/L (10 mL)	Nb-hematite $Fe_{2-x}Nb_xO_3$ (10 g/L)	0.3 mol/L	6.0	25	–	Low discoloration with pure hematite and Hm-Nb_2, 70% color removal, and 25% TOC removal after 60 min with Hm-Nb10	Silva et al. (2009)
Methylene blue [MB], 50 mg/L (10 mL)	Nb-hematite-maghemite treated by H_2O_2 (1 g/L)	8.0 mM 30% v/v	6.0	25	–	73% MB removal using treated catalyst compared to 30% MB removal by non-treated samples within 60 min	Silva et al. (2011)

Bromophenol blue, Chicago sky blue, Evans blue and Naphthol blue black [dye] 50 mg/	FeO-Fe_2O_3 (25 mg/mL)	100 mmol/L	6.6	30	–	90% color removal within 24 h, the fast decomposition rate at first hour	Baldrian et al. (2006)
Naphthol blue black [NBB] 500 mg/L, COD_0 1.80	MO-Fe_2O_3 (M: Mn, Co, Cu, Fe) 25 mg/mL	100 mmol/L	6.0–6.6	30	–	COD removal of 97%, 92%, 88%, and 75% and color removal of 85%, 67%, 53%, and 58% using the catalysts of Cu, Co, Fe, and Mn, respectively	Baldrian et al. (2006)
Dimethyl phthalate [DMP] 7.7 mg/L (100 mL)	Si-FeOOH 0.5 g L^{-1}	2 mmol/L	5.0	25	365	97% DMP degradation within 30 min	Yuan et al. (2011)
Methylene blue [MB] 50 mg/L	Nb-FeOOH (11% Nb) 1 g/L	0.3 mol/L	6.0	25	–	15% discoloration after 120 min by pure goethite, ≈ 85% color removal using Nb11-FeOOH within 120 min	Oliveira et al. (2008)
Quinoline [Q] 10 mg/L	Ni-FeOOH 1 g/L	0.1 mL 5% v/v	6.0	25	–	28% Q removal after 5 h by pure goethite, 70% Q removal within 5 h	de Souza et al. (2010)

The optimum transition metal content generally decreases the crystal size significantly, with concomitant increased specific surface area, leading to the higher capacities for the adsorption in the samples. Despite the good adsorption efficiencies of the modified magnetite, it incapacitates in contaminant degradation. Consequently, hydrogen peroxide was introduced to the system that in turn hydroxyl radicals were generated through catalytic action of iron/imported transition metals in the magnetite. These generated hydroxyl radicals are highly energetic to attack the pollutant molecules and oxidize them to water and carbon dioxide.

Finally, for further discovery and understanding this class of catalysts, exploring the best combinations for higher degradation efficiencies and investigation of the effects of various factors such as wastewater composition on the stability, lixiviation, and aging of the catalytic sites for longer and efficient use in Fenton treatment of recalcitrant wastewaters are recommended.

References

Ai L, Zhang C, Liao F, Wang Y, Li M, Meng L, Jiang J (2011a) Removal of methylene blue from aqueous solution with magnetite loaded multi-wall carbon nanotube: kinetic, isotherm and mechanism analysis. J Hazard Mater 198:282–290

Ai L, Zhang C, Meng L (2011b) Adsorption of methyl orange from aqueous solution on hydrothermal synthesized Mg–Al layered double hydroxide. J Chem Eng Data 56:4217–4225

Ali I (2012) New generation adsorbents for water treatment. Chem Rev 112:5073–5091

Ali I, Jain CK (2005) Wastewater treatment and recycling technologies. Water encyclopedia. Wiley, New York

Ali I, Gupta VK (2007) Advances in water treatment by adsorption technology. Nat Protoc 1:2661–2667

Alvarez M, Rueda EH, Sileo EE (2006) Structural characterization and chemical reactivity of synthetic Mn-goethites and hematites. Chem Geol 23:288–299

Anirudhan TS, Shainy F (2015) Adsorption behaviour of 2-mercaptobenzamide modified itaconic acid-grafted-magnetite nanocellulose composite for cadmium(II) from aqueous solutions. J Ind Eng Chem 32:157–166

Baldrian P, Merhautová V, Gabriel J, Nerud F, Stopka P, Hrubý M, Beneš MJ (2006) Decolorization of synthetic dyes by hydrogen peroxide with heterogeneous catalysis by mixed iron oxides. Appl Catal B-Environ 66:258–264

Bhattacharya A, Arun K, Venkobachar C (1984) Removal of cadmium (II) by low cost adsorbents. J Environ Eng 110:110–122

Büchler M, Schmuki P, Böhni H, Stenberg T, Mäntilä T (1998) Comparison of the semiconductive properties of sputter-deposited iron oxides with the passive film on iron. J Electrochem Soc 145:378–385

Choi J, Chung J, Lee W, Kim JO (2016) Phosphorous adsorption on synthesized magnetite in wastewater. J Ind Eng Chem 34:198–203

Coker VS, Pearce CI, Pattrick RAD, van der Laan G, Telling ND, Charnock JM, Arenholz E, Lloyd JR (2008) Probing the site occupancies of Co-, Ni-, and Mn-substituted biogenic magnetite using XAS and XMCD. Am Mineral 93:1119–1132

Comninellis C, Kapalka A, Malato S, Parsons SA, Poulios I, Mantzavinos D (2008) Perspective, advanced oxidation processes for water treatment: advances and trends for R&D. J Chem Technol Biot 83:769–776

Cornell RM, Schwertmann U (2003) The iron oxides: structure, properties, reactions, occurrences and uses. Wiley, Weinheim

Costa RCC, Lelis MFF, Oliveira LCA, Fabris JD, Ardisson JD, Rios RRVA, Silva CN, Lago RM (2003) Remarkable effect of Co and Mn on the activity of $Fe_{3-x}M_xO_4$ promoted oxidation of organic contaminants in aqueous medium with H_2O_2. Catal Commun 4:525–529

Costa RC, Lelis MFF, Oliveira LCA, Fabris JD, Ardisson JD, Rios RRVA, Silva CN, Lago RM (2006) Novel active heterogeneous Fenton system based on $Fe_{3-x}M_xO_4$ (Fe, Co, Mn, Ni): the role of M^{2+} species on the reactivity towards H_2O_2 reactions. J Hazard Mater 129:171–178

de Souza WF, Guimarães IR, Oliveira LCA, Giroto AS, Guerreiro MC, Silva CLT (2010) Effect of Ni incorporation into goethite in the catalytic activity for the oxidation of nitrogen compounds in petroleum. Appl Catal A-Gen 381:36–41

Delmas H, Creanga C, Julcour-Lebigue C, Wilhelm AM (2009) AD–OX: a sequential oxidative process for water treatment – adsorption and batch CWAO regeneration of activated carbon. Chem Eng J 152:189–194

Diya'uddeen BH, Rahim Pouran S, Abdul Aziz AR, Nashwan SM, Wan Daud WMA, Shaaban MG (2015a) Hybrid of Fenton and sequencing batch reactor for petroleum refinery wastewater treatment. J Ind Eng Chem 25:186–191

Diya'uddeen BH, Rahim Pouran S, Abdul Aziz AR, Daud WMAW (2015b) Fenton oxidative treatment of petroleum refinery wastewater: process optimization and sludge characterization. RSC Adv 5:68159–68168

dos Santos CA, Horbe AMC, Barcellos CMO, Marimon da Cunha JB (2001) Some structure and magnetic effects of Ga incorporation on α-FeOOH. Solid State Commun 118:449–452

Guimaraes IR, Giroto A, Oliveira LC, Guerreiro MC, Lima DQ, Fabris JD (2009) Synthesis and thermal treatment of cu-doped goethite: oxidation of quinoline through heterogeneous fenton process. Appl Catal B-Environ 91:581–586

Guyo U, Makawa T, Moyo M, Nharingo T, Nyamunda BC, Mugadza T (2015) Application of response surface methodology for Cd (II) adsorption on maize tassel-magnetite nanohybrid adsorbent. J Environ Chem Eng 3:2472–2483

Haneda K, Morrish AH (1988) Noncollinear magnetic structure of CoFe2O4 small particles. J Appl Phys 63:4258–4260

Hanna K, Kone T, Medjahdi G (2008) Synthesis of the mixed oxides of iron and quartz and their catalytic activities for the Fenton-like oxidation. Catal Commun 9:955–959

Herney-Ramirez J, Vicente MA, Madeira LM (2010) Heterogeneous photo-Fenton oxidation with pillared clay-based catalysts for wastewater treatment: a review. Appl Catal B-Environ 98:10–26

Ho YS, McKay G (1999) Pseudo-second order model for sorption processes. Process Biochem 34:451–465

Hua M, Zhang S, Pan B, Zhang W, Lv L, Zhang Q (2012) Heavy metal removal from water/wastewater by nanosized metal oxides: a review. J Hazard Mater 211:317–331

Jentzsch TL, Lan Chun C, Gabor RS, Lee PR (2007) Influence of aluminum substitution on the reactivity of magnetite nanoparticles. J Phys Chem C 111:10247–10253

Lagergren S (1898) About the theory of so-called adsorption of soluble substances. K Sven Vetenskapsakad Handl 24:1–39

Lasheen MR, El-Sherif IY, Tawfik ME, El-Wakeel ST, El-Shahat MF (2016) Preparation and adsorption properties of nano magnetite chitosan films for heavy metal ions from aqueous solution. Mater Res Bull 80:344–350

Lee CS, Joe YH (2010) Structural and magnetic properties of cu-substituted magnetite studied by using Mössbauer spectroscopy. J Korean Phys Soc 56:85–88

Lee HJ, Kim G, Kim DH, Kang JS, Zhang CL, Cheong SW, Shim JH, Lee S, Lee H, Kim JY, Kim BH, Min BI (2008) Valence states and occupation sites in $(Fe, Mn)_3O_4$ spinel oxides investigated by soft x-ray absorption spectroscopy and magnetic circular dichroism. J Phys Condens Matter 20:295–303

Lelis MFF, Porto AO, Gonçalves CM, Fabris JD (2004) Cation occupancy sites in synthetic Co-doped magnetites as determined with X-ray absorption (XAS) and Mössbauer spectroscopies. J Magn Magn Mater 278:263–269

Liang X, Zhu S, Zhong Y, Zhu J, Yuan P, He H, Zhang J (2010) The remarkable effect of vanadium doping on the adsorption and catalytic activity of magnetite in the decolorization of methylene blue. Appl Catal B-Environ 97:151–159

Liang X, Zhong Y, He H, Yuan P, Zhu J, Zhu S, Jiang Z (2012a) The application of chromium substituted magnetite as heterogeneous Fenton catalyst for the degradation of aqueous cationic and anionic dyes. Chem Eng J 191:177–184

Liang X, Zhong Y, Zhu S, Ma L, Yuan P, Zhu J, He H, Jiang Z (2012b) The contribution of vanadium and titanium on improving methylene blue decolorization through heterogeneous UV-Fenton reaction catalyzed by their co-doped magnetite. J Hazard Mater 199:247–254

Liang X, He Z, Zhong Y, Tan W, He H, Yuan P, Zhu J, Zhang J (2013) The effect of transition metal substitution on the catalytic activity of magnetite in heterogeneous Fenton reaction: in interfacial view. Colloid Surface A 435:28–35

Liang X, He Z, Wei G, Liu P, Zhong Y, Tan W, Du P, Zhu J, He H, Zhang J (2014) The distinct effects of Mn substitution on the reactivity of magnetite in heterogeneous Fenton reaction and Pb(II) adsorption. J Colloid Interface Sci 426:181–189

Magalhães F, Pereira MC, Botrel SEC, Fabris JD, Macedo WA, Mendonca R, Lago RM, Oliveira LCA (2007) Cr-containing magnetites $Fe_{3-x}Cr_xO_4$: the role of Cr^{3+} and Fe^{2+} on the stability and reactivity towards H_2O_2 reactions. Appl Catal A-Gen 332:115–123

Malato S, Fernández-Ibáñez P, Maldonado MI, Blanco J, Gernjak W (2009) Decontamination and disinfection of water by solar photocatalysis: recent overview and trends. Catal Today 147:1–59

Moura FCC, Oliveira GC, Araujo MH, Ardisson JD, Macedo WAA, Lago RM (2006) Highly reactive species formed by interface reaction between Fe0–iron oxides particles: an efficient electron transfer system for environmental applications. Appl Catal A-Gen 307:195–204

Munoz M, de Pedro ZM, Casas JA, Rodriguez JJ (2015) Preparation of magnetite-based catalysts and their application in heterogeneous Fenton oxidation – a review. Appl Catal B-Environ 176:249–265

Nichela DA, Berkovic AM, Costante MR, Juliarena MP, García FSE (2013) Nitrobenzene degradation in Fenton-like systems using Cu(II) as catalyst. Comparison between Cu(II) – and Fe(III)-based systems. Chem Eng J 228:1148–1157

Nitoi I, Oncescu T, Oancea P (2013) Mechanism and kinetic study for the degradation of lindane by photo-Fenton process. J Ind Eng Chem 19:305–309

Oliveira LCA, Lago RM, Rios RVRA, Augusti R, Sousa PP, Mussel WN, Fabris JD (2000) The effect of Mn substitution on the catalytic properties of ferrites. Stud Surf Sci Catal 130:2165–2170

Oliveira LCA, Gonçalves M, Guerreiro MC, Ramalho TC, Fabris JD, Pereira MC, Sapag K (2007) A new catalyst material based on niobia/iron oxide composite on the oxidation of organic contaminants in water via heterogeneous Fenton mechanisms. Appl Catal A-Gen 316:117–124

Oliveira LCA, Ramalho TC, Souza EF, Gonçalves M, Oliveira DQM, Pereira MC, Fabris JD (2008) Catalytic properties of goethite prepared in the presence of Nb on oxidation reactions in water: computational and experimental studies. Appl Catal B-Environ 83:169–176

Pearce CI, Henderson CMB, Telling ND, Pattrick RAD, Charnock JM, Coker VS, Arenholz E, Tuna F, Van der Laan G (2015) Fe site occupancy in magnetite-ulvöspinel solid solutions: a new approach using X-ray magnetic circular dichroism. Am Mineral 95:425–439

Petrova TM, Fachikov L, Hristov J (2011) The magnetite as adsorbent for some hazardous species from aqueous solutions: a review. Int Rev Chem Eng 3:134–152

Pignatello JJ, Oliveros E, MacKay A (2006) Advanced oxidation processes for organic contaminant destruction based on the Fenton reaction and related chemistry. Crit Rev Environ Sci Technol 36:1–84

Rahim Pouran S, Abdul Raman AA, Wan Daud WMA (2014) Review on the application of modified iron oxides as heterogeneous catalysts in Fenton reactions. J Clean Prod 64:24–35

Rahim Pouran S, Abdul Aziz AR, Wan Daud WMA, Embong Z (2015a) Niobium substituted magnetite as a strong heterogeneous Fenton catalyst for wastewater treatment. Appl Surf Sci 351:175–187

Rahim Pouran S, Abdul Aziz AR, Wan Daud WMA (2015b) Review on the main advances in photo-Fenton oxidation system for recalcitrant wastewaters. J Ind Eng Chem 21:53–69

Rahim Pouran S, Abdul Aziz AR, Wan Daud WMA, Shafeeyan MS (2015c) Effects of niobium and molybdenum impregnation on adsorption capacity and Fenton catalytic activity of magnetite. RSC Adv 5:87535–87549

Rajput S, Pittman CU Jr, Mohan D (2016) Magnetic magnetite (Fe_3O_4) nanoparticle synthesis and applications for lead (Pb^{2+}) and chromium (Cr^{6+}) removal from water. J Colloid Interface Sci 468:334–346

Ramankutty CG, Sugunan S (2002) Surface properties and catalytic activity of ferrospinels of nickel, cobalt and copper, prepared by soft chemical methods. Appl Catal A-Gen 218:39–51

Shestakova M, Vinatoru M, Mason TJ, Sillanpää M (2015) Sonoelectrocatalytic decomposition of methylene blue using Ti/Ta_2O_5–SnO_2 electrodes. Ultrason Sonochem 23:135–141

Shukla P, Wang S, Sun H, Ang HM, Tadé M (2010) Adsorption and heterogeneous advanced oxidation of phenolic contaminants using Fe loaded mesoporous SBA-15 and H_2O_2. Chem Eng J 164:255–260

Silva AC, Oliveira DQL, Oliveira LCA, Anastácio AS, Ramalho TC, Lopes JH, Carvalho HWP, Rodrigues Torres CE (2009) Nb-containing hematites $Fe_{2-x}Nb_xO_3$: the role of Nb^{5+} on the reactivity in presence of the H_2O_2 or ultraviolet light. Appl Catal A-Gen 357:79–84

Silva AC, Cepera RM, Pereira MC, Lima DQ, Fabris JD, Oliveira LCA (2011) Heterogeneous catalyst based on peroxo-niobium complexes immobilized over iron oxide for organic oxidation in water. Appl Catal B-Environ 107:237–244

Sugimoto T, Matijević E (1980) Formation of uniform spherical magnetite particles by crystallization from ferrous hydroxide gels. J Colloid Interface Sci 74:227–243

Sun ZX, Su FW, Forsling W, Samskog PO (1998) Surface characteristics of magnetite in aqueous suspension. J Colloid Interface Sci 197:151–159

Wang JL, Xu LJ (2011) Advanced oxidation processes for wastewater treatment: formation of hydroxyl radical and application. Crit Rev Environ Sci Technol 42:251–325

Yang S, He H, Wu D (2009a) Decolorization of methylene blue by heterogeneous Fenton reaction using $Fe_{3-x}Ti_xO_4$ ($0 \leq x \leq 0.78$) at neutral pH values. Appl Catal B-Environ 89:527–535

Yang S, He H, Wu D, Chen D, Ma Y, Li X, Zhu J, Yuan P (2009b) Degradation of methylene blue by heterogeneous Fenton reaction using titanomagnetite at neutral pH values: process and affecting factors. Ind Eng Chem Res 48:9915–9921

Yuan P, Fan M, Yang D, He H, Lui D, Yuan A, Zhu J, Chen T (2009) Montmorillonite-supported magnetite nanoparticles for the removal of hexavalent chromium [Cr(VI)] from aqueous solutions. J Hazard Mater 166:821–829

Yuan B, Li X, Li K, Chen W (2011) Degradation of dimethyl phthalate (DMP) in aqueous solution by UV/Si–FeOOH/H_2O_2. Colloid Surf A 379:157–162

Zhong Y, Liang X, Zhong Y, Zhu J, Zhu S, Yuan P, He H, Zhang J (2012) Heterogeneous UV/Fenton degradation of TBBPA catalyzed by titanomagnetite: catalyst characterization, performance and degradation products. Water Res 46:4633–4644